

Introduction

Determining lifetime-accumulated radiation dose is increasingly viewed as essential. Computational phantoms containing dosimetric information, e.g. the extended cardiac-torso (XCAT) phantom [2], are being developed, but they cannot adequately reflect variability between patients, especially for growing children. Here, custom phantoms are made by manually segmenting a small set of organs from CT and calculating a full-body registration to an adult XCAT [3] using large deformation diffeomorphic metric mapping (LDDMM). The result is used to map anatomical and dosimetric data to the child (Fig. 1).

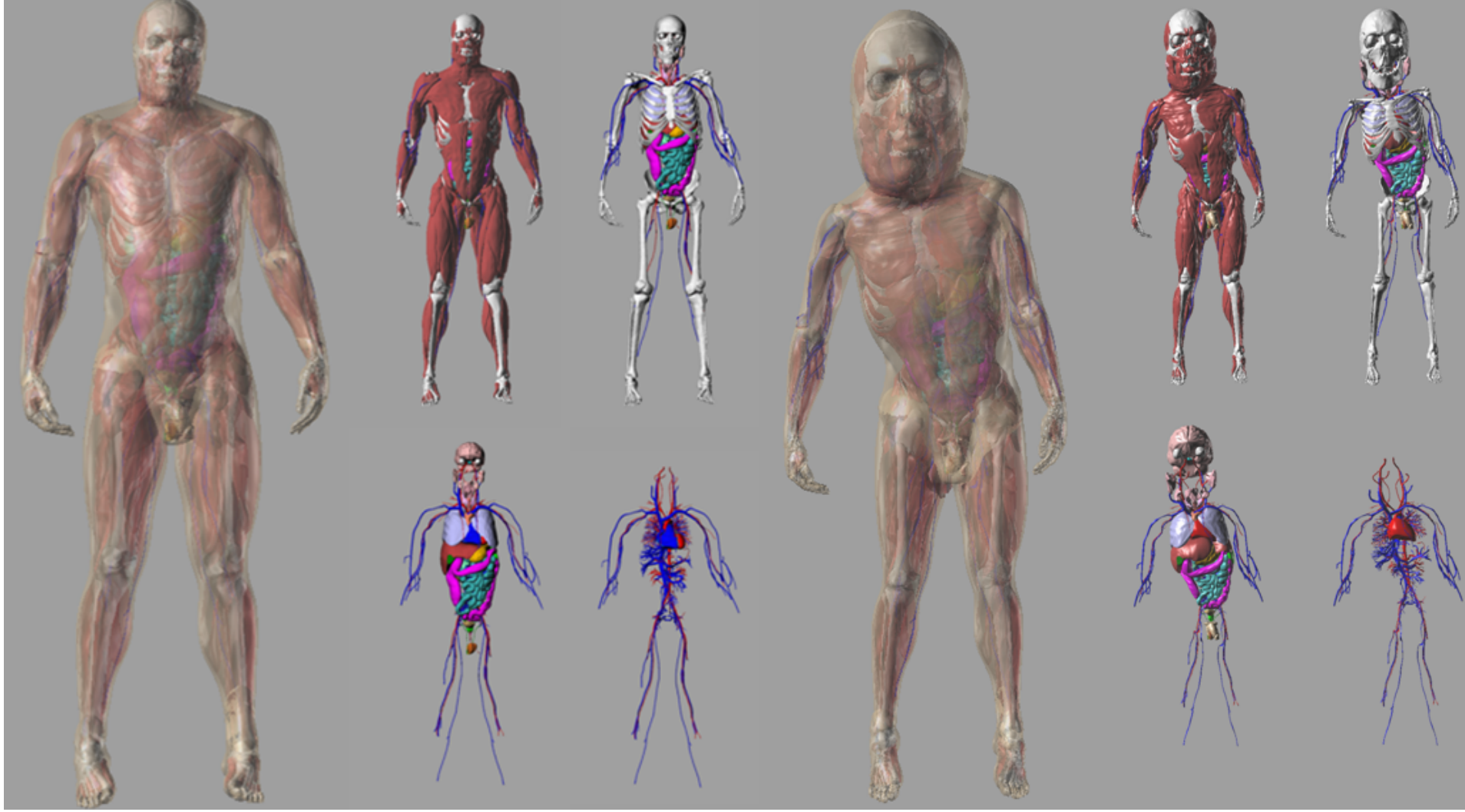


Figure 1. The adult XCAT phantom (left) and customized pediatric phantom (right) are shown with transparency and built up progressively from anatomical systems.

Methods

Full body mapping. We generated mappings between one of two adult templates (male, female), and pediatric patients (24 male, 18 female) defined on a $256 \times 256 \times 520$ 2mm^3 voxel grid. Patients' volume varied between 0.072 and 0.472 (mean 0.233) that of the adult. Images were segmented into 8 organs (body, bones, brain, lungs, liver, kidneys, stomach, spleen), and 87 landmarks were placed automatically [2] mainly on reproducible bony structures. Images were initially aligned based on landmarks, linearly then deformably. Multi-channel (MC) LDDMM, which treats each organ as a separate image on a common background space [1], was used to create dense mappings. To achieve robustness on this variable dataset, a coarse to fine strategy was adopted. MC-LDDMM was run four times with decreasing regularization in a manner that remains numerically stable, the final regularization being specified by the desired accuracy. This sequence of transformations is shown in Fig. 2. This modification leads to increased computation time, and as such parallelization of the algorithm was analyzed. A subset of four patients was chosen for which mapping was repeated on 1, 2, 4, 8, 16, and 24 processors.

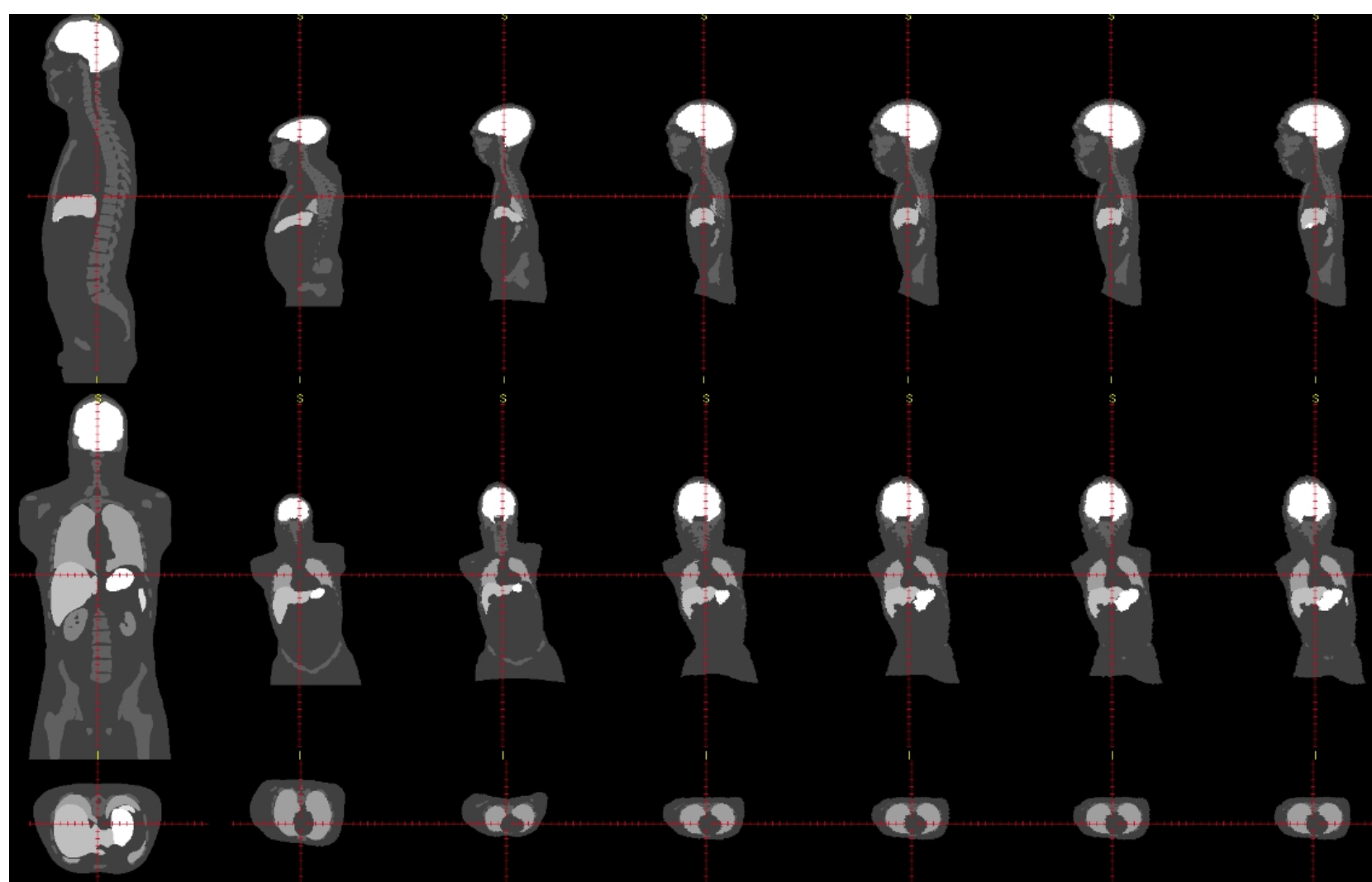


Figure 2. The robust sequence of transformations used. Top to bottom: sagittal, coronal, and axial slices. Left to right: initial placement, affine registration, LDDMM landmark, 1 - 4 iterations of MC-LDDMM

MC-LDDMM. The desired transformation minimizes the following over smooth velocity fields \mathbf{v}_t

$$E = \int dt \|\mathbf{L}\mathbf{v}_t\|_2^2 + \sum_{i=1}^M \frac{1}{\sigma_i^2} \|\mathbf{I}_0^i \circ \phi_{t=1}^{-1} - \mathbf{I}_1^i\|_2^2 \quad (1)$$

where, \mathbf{I}_1^i and \mathbf{I}_0^i are the i^{th} (of M) organs of the target and template, $\phi_{t=1}$ is a diffeomorphism generated by integrating \mathbf{v}_t from $t = 0$ to 1 , and σ_i^2 describes the contribution of the i^{th} channel to the overall energy. The operator $\mathbf{L} = -\gamma \mathbf{Id} + \alpha \nabla^2$ where $\gamma = -1$ is fixed and α is varied, \mathbf{Id} is identity and ∇^2 is the Laplacian operator, ensures smoothness of the velocity field and resulting deformations, with larger α for smoother (more regular) deformations, and smaller α for more accurate transformations. We use a gradient descent strategy, and the energy gradient can be computed as [1]

$$\nabla_{\mathbf{v}} E_t = 2\mathbf{v}_t - \mathbf{K} \left[\sum_{i=1}^M \frac{2}{\sigma_i^2} |D\phi_{t,1}| \nabla J_t^{0i} (J_t^{0i} - J_t^{1i}) \right], \quad (2)$$

where \mathbf{K} is the operator inverse of $\mathbf{L}^T \mathbf{L}$, $|\cdot|$ denotes determinant, D denotes the Jacobian, and ∇ the spatial gradient. The transformation generated by integrating \mathbf{v}_t from time $t' = s$ to time $t' = t$ is denoted $\phi_{s,t}$. The quantity J_t^{0i} is the i^{th} template channel transformed up to time t ($= \mathbf{I}_0^i \circ \phi_{t,0}$), and J_t^{1i} is the i^{th} target channel transformed backwards from time 1 to time t ($= \mathbf{I}_1^i \circ \phi_{t,1}$).

References

- [1] C. Ceritoglu et al. Multi-contrast large deformation diffeomorphic metric mapping for diffusion tensor imaging. *Neuroimage*, 47: 618-627, 2009.
- [2] W. P. Segars et al. Realistic CT simulation using the 4D XCAT phantom. *Medical Physics*, 35:3800-3808, 2008.
- [3] W. P. Segars et al. Patient specific computerized phantoms to estimate dose in pediatric CT. *Proceedings of SPIE Medical*

1. Center for Imaging Sciences, Johns Hopkins University, Baltimore, MD
2. Carl E. Ravin Advanced Imaging Laboratories, Duke University, Durham, NC
3. Department of Biomedical Engineering, University of North Carolina, Chapel Hill, NC
4. Department of Radiology, Duke University Medical Center, Durham, NC
5. Institute for Computational Medicine, The Johns Hopkins University, Baltimore, MD

Results

Transformations and phantoms. An example of the transformed organs used for MC-LDDMM are shown as isosurfaces in Fig. 3. The result of the full body mapping algorithm for the same pediatric patient is illustrated in the transformation between the left and right side of Fig. 1.

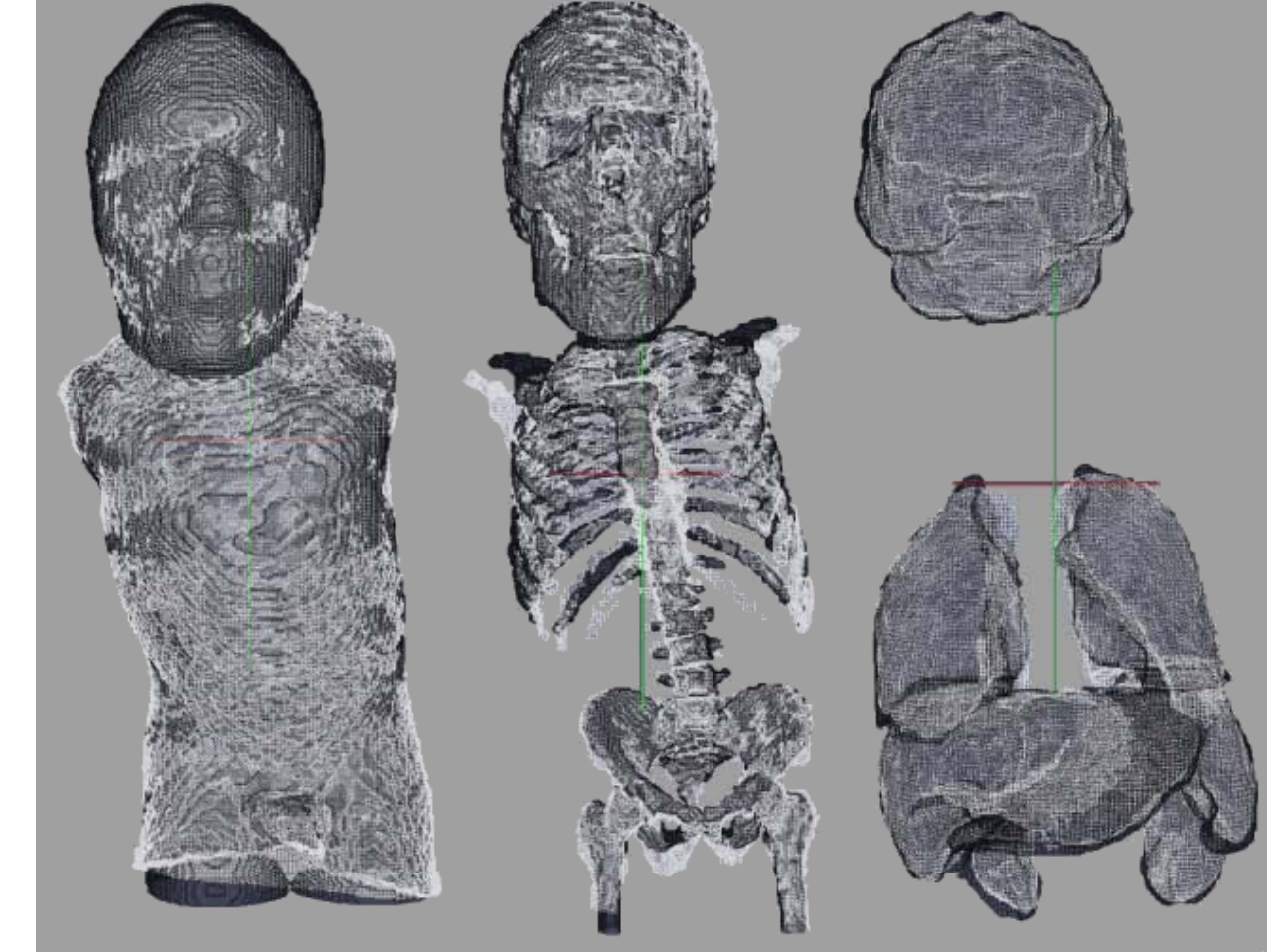


Figure 3. Triangulated surfaces from an example deformed adult template (white) and target child (black).

Accuracy. Accuracy of mappings was quantified by measuring surface to surface distance at each vertex along isosurfaces. Cumulative distributions are shown in Fig. 4, grouped into males and females, organ by organ (brain is matched with the most fidelity and stomach with the least), and patient by patient (accuracy for females is more variable). The algorithm is accurate typically to within 1-2 voxels (2-4 mm), and robust across this large and variable data set

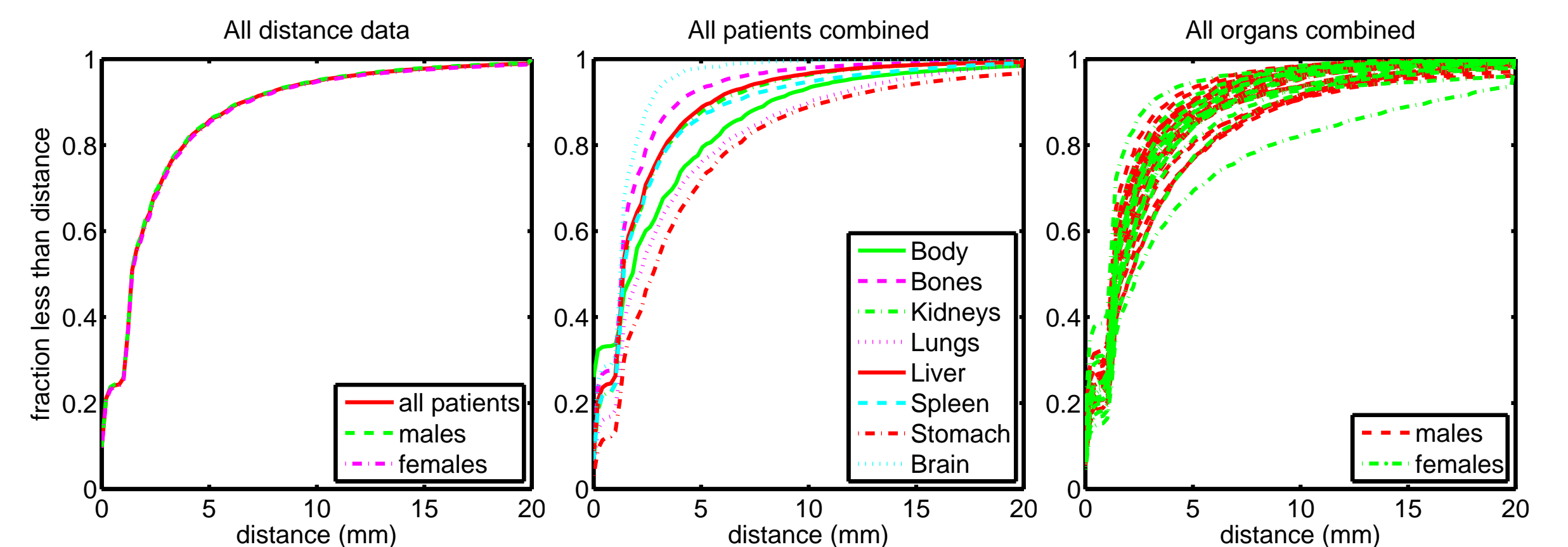


Figure 4. Surface to surface distance cumulative distribution functions are shown to demonstrate the accuracy of full body mapping. Left to right, separated by gender, separated by organ, separated by individual patient.

Computational performance. The four patients examined for quantification of efficiency are denoted “small”, “med-small”, “med-large”, and “large”. The total computational time in hours, excluding input/output (IO) operations, is shown in Table 1. Parallelization allows computation time to be reduce from over a day, to only a few hours.

Table 1. Total timing (in hours) excluding IO operations

Processors	1	2	4	8	16	24
Small	8.94	4.9	2.62	1.49	1.06	0.935
Med-Small	33.5	18.2	9.68	5.41	3.64	3.25
Med-Large	31.3	17.3	9.05	5.07	3.5	3.17
Large	28	15.2	7.92	4.47	3.1	2.8

The speedup factor and efficiency of parallelization are shown in Fig 5. 93.84% of the algorithm is effectively parallelized, and efficiency remains high until beyond 8 processors are used.

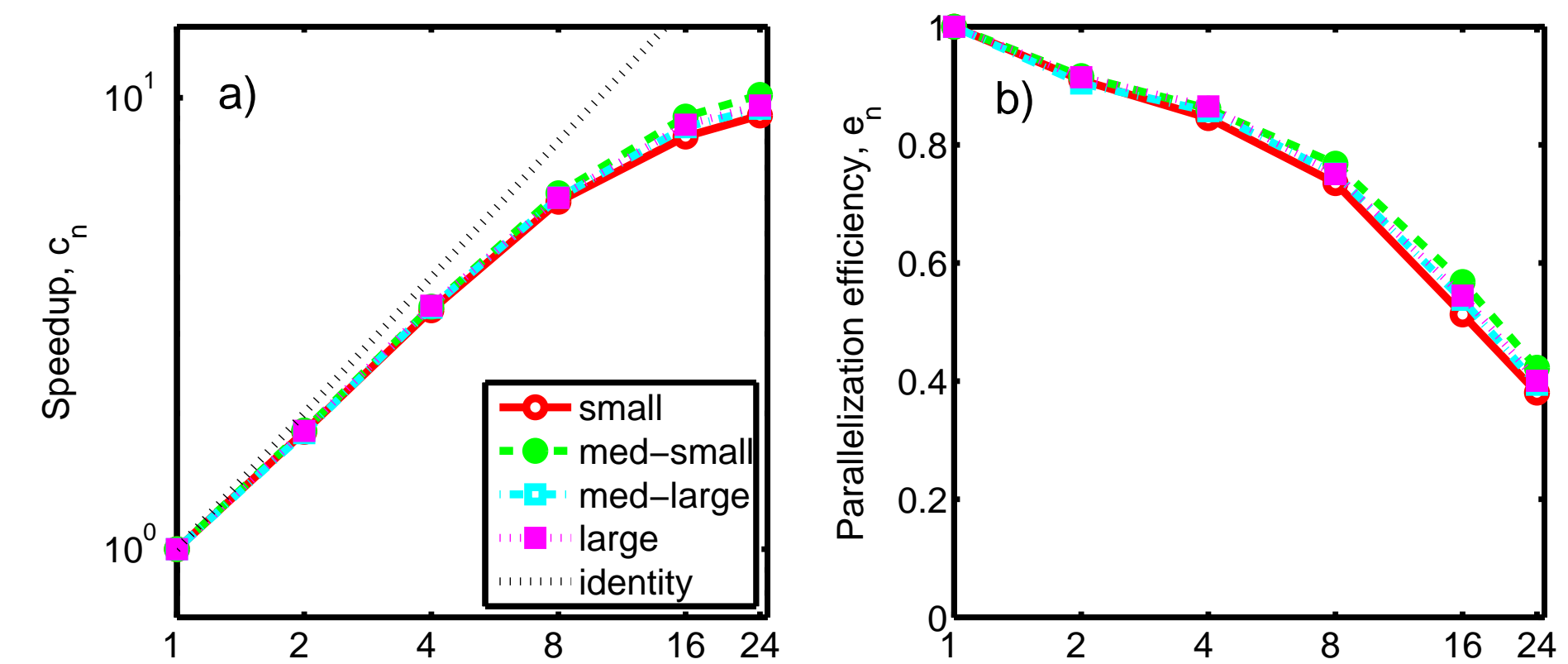


Figure 5. a) Speedup due to parallelization (log scale), and b) efficiency of parallelization (semilog scale), for the four patients examined.

Conclusion

The algorithm used here for generating full body maps involves a sequence of increasingly detailed transformations between adult templates and child images. This procedure ensures the robustness necessary to automate calculations across a wide range of pediatric patients. It comes at the price of high computational cost, which fortunately can be mitigated with a parallel implementation. This algorithm takes advantage of a powerful feature of diffeomorphisms. Their submanifold preserving property allows a transformation calculated from a handful of segmented (Fig. 3) structures to be accurately and smoothly applied to the thousands of anatomical structures defined in the XCAT phantom (Fig. 1).